HIF1α Suppresses Tumor Cell Proliferation through Inhibition of Aspartate Biosynthesis

Graphical Abstract

Highlights

- HIF1α reduces intracellular aspartate levels

- HIF1α impairs oxidative and reductive aspartate biosynthesis

- The aspartate-generating GOT1 and GOT2 enzymes are repressed by HIF1α

- Aspartate supplementation counteracts the antiproliferative influence of HIF1α

Authors

Florinda Meléndez-Rodríguez,
Andrés A. Urrutia, Doriane Lorendeau, ...,
Sarah-Maria Fendt, Katrien De Bock,
Julián Aragonés

Correspondence

jaragones.hlpr@salud.madrid.org

In Brief

Meléndez-Rodríguez et al. show that HIF1α impairs oxidative and reductive aspartate biogenesis, which consequently drives HIF1α-dependent suppression of tumor cell proliferation. Mechanistically, HIF1α represses the aspartate-producing enzymes GOT1 and GOT2 in several biological settings, including human VHL-deficient renal cell carcinoma, in which HIF1α can act as a tumor suppressor.

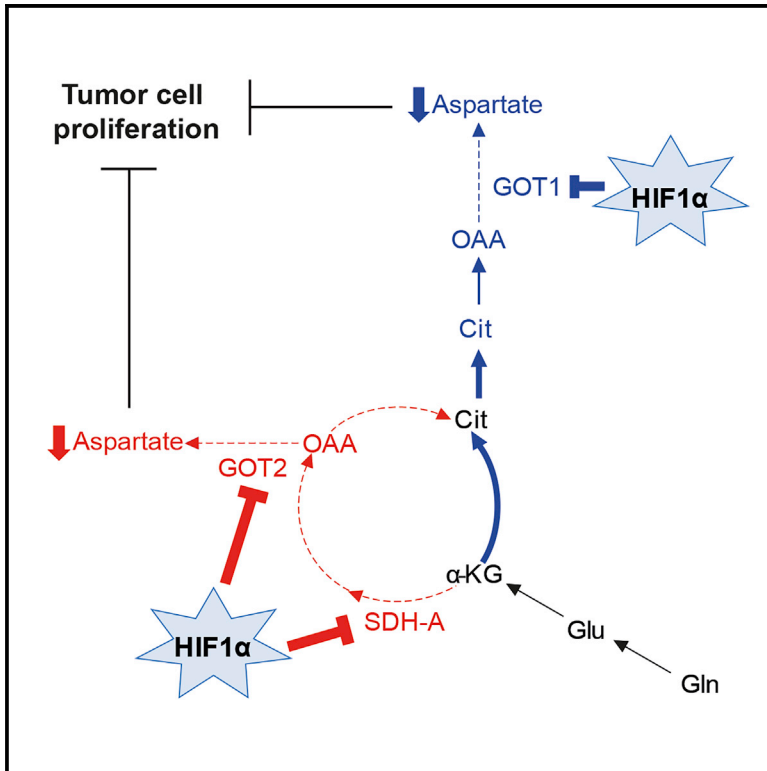# HIF1α Suppresses Tumor Cell Proliferation through Inhibition of Aspartate Biosynthesis

Florinda Meléndez-Rodríguez,[1,2,14] Andrés A. Urrutia,[1,14] Doriane Lorendeau,[4,5] Gianmarco Rinaldi,[4,5] Olga Roche,[7,8] Nuray Bögürcü-Seidel,[9] Marta Ortega Muelas,[8] Claudia Mesa-Ciller,[1] Guillermo Turiel,[1] Antonio Bouthelier,[1] Pablo Hernansanz-Agustín,[1] Ainara Elorza,[1] Elia Escasany,[1] Qilong Oscar Yang Li,[1] Mar Torres-Capelli,[1] Daniel Tello,[1] Esther Fuertes,[1] Enrique Fraga,[1] Antonio Martínez-Ruiz,[1,2] Belen Pérez,[11,12] Jose Miguel Giménez-Bachs,[10] Antonio S. Salinas-Sánchez,[10] Till Acker,[9] Ricardo Sánchez Prieto,[6,7] Sarah-Maria Fendt,[4,5] Katrien De Bock,[3] and Julián Aragonés[1,2,13,*]

[1]Research Unit, Hospital of Santa Cristina, Research Institute Princesa (IP), Autonomous University of Madrid, Madrid 28009, Spain
[2]CIBER de Enfermedades Cardiovasculares (CIBERCV), Carlos III Health Institute, Madrid, Spain
[3]Department of Health Sciences and Technology, Swiss Federal Institute of Technology (ETH), Zurich, Switzerland
[4]Laboratory of Cellular Metabolism and Metabolic Regulation, VIB Center for Cancer Biology, VIB, Herestraat 49, 3000 Leuven, Belgium
[5]Laboratory of Cellular Metabolism and Metabolic Regulation, Department of Oncology, KU Leuven and Leuven Cancer Institute (LKI), Herestraat 49, 3000 Leuven, Belgium
[6]Departamento de Biología del Cáncer, Instituto de Investigaciones Biomédicas Alberto Sols (CSIC-UAM), Unidad Asociada de Biomedicina UCLM, Unidad Asociada al CSIC, Madrid, Spain
[7]Departamento de Ciencias Médicas, Facultad de Medicina de Albacete, Universidad de Castilla-La Mancha, Albacete, Spain
[8]Laboratorio de Oncología, Unidad de Medicina Molecular, Centro Regional de Investigaciones Biomédicas/UCLM, Unidad Asociada de Biomedicina UCLM-CSIC, 02006 Albacete, Spain
[9]Institute of Neuropathology, University of Giessen, Giessen, Germany
[10]Servicio de Urología, Complejo Hospitalario Universitario de Albacete, Facultad de Medicina de la UCLM, Albacete, Spain
[11]Centro de Diagnóstico de Enfermedades Moleculares, Centro de Biología Molecular-SO UAM-CSIC, Universidad Autónoma de Madrid, 28049 Madrid, Spain
[12]CIBERER, Madrid, IdiPaz, Spain
[13]Lead Contact
[14]These authors contributed equally
*Correspondence: jaragones.hlpr@salud.madrid.org
https://doi.org/10.1016/j.celrep.2019.01.106

SUMMARY

Cellular aspartate drives cancer cell proliferation, but signaling pathways that rewire aspartate biosynthesis to control cell growth remain largely unknown. Hypoxia-inducible factor-1α (HIF1α) can suppress tumor cell proliferation. Here, we discovered that HIF1α acts as a direct repressor of aspartate biosynthesis involving the suppression of several key aspartate-producing proteins, including cytosolic glutamic-oxaloacetic transaminase-1 (GOT1) and mitochondrial GOT2. Accordingly, HIF1α suppresses aspartate production from both glutamine oxidation as well as the glutamine reductive pathway. Strikingly, the addition of aspartate to the culture medium is sufficient to relieve HIF1α-dependent repression of tumor cell proliferation. Furthermore, these key aspartate-producing players are specifically repressed in VHL-deficient human renal carcinomas, a paradigmatic tumor type in which HIF1α acts as a tumor suppressor, highlighting the *in vivo* relevance of these findings. In conclusion, we show that HIF1α inhibits cytosolic and mitochondrial aspartate biosynthesis and that this mechanism is the molecular basis for HIF1α tumor suppressor activity.

INTRODUCTION

The biosynthesis of aspartate is central in cancer cell autonomous proliferation because it is essential not only for protein synthesis but also for nucleotide biosynthesis in proliferating cells (Birsoy et al., 2015; Lane and Fan, 2015; Sullivan et al., 2015). Circulating levels of aspartate are low compared with other amino acids (Mayers and Vander Heiden, 2015), and it is presumed that most cells largely rely on intracellular aspartate biosynthesis to sustain cellular growth. Aspartate biosynthesis is driven largely by glucose- or glutamine-dependent refilling of the tricarboxylic acid (TCA) cycle to replenish mitochondrial TCA intermediate oxaloacetate, which is subsequently converted to aspartate through the activity of mitochondrial glutamic-oxaloacetic transaminase (GOT2). Alternatively, cells can also use reductive glutamine metabolism to generate aspartate through the cytosolic GOT1 isoform (Birsoy et al., 2015). This function of GOT1 is relevant to sustain aspartate biosynthesis and cell proliferation when mitochondrial-dependent aspartate biosynthesis is compromised (Birsoy et al., 2015). However, the intracellular signals that rewire aspartate biosynthesis to attenuate cell growth remain largely unknown.

Hypoxia-inducible factors (HIFs) are key transcriptional regulators of the adaptive tumor cellular response to low oxygen tension. Under normoxic conditions, critical key proline residues in HIFα subunits are hydroxylated by prolyl hydroxylases (PHD1–3), which ultimately leads to their recognition by the von Hippel-Lindau (VHL) protein and their consequent degradation by the

proteasome (Epstein et al., 2001; Ivan et al., 2001; Jaakkola et al., 2001; Wang et al., 1995). In hypoxic conditions, PHD activity is restrained, and therefore VHL is unable to recognize HIFα subunits, leading to their nuclear accumulation. HIF1α can act as a repressor of tumor cell proliferation in different biological settings (Carmeliet et al., 1998; Gordan et al., 2007; Hubbi et al., 2013) and has been widely studied in clear cell renal cell carcinoma (CCRCC), which is characterized by VHL inactivation and consequent constitutive normoxic activation of the HIF1α (Gordan et al., 2007; Kaelin, 2008). In this line, a large proportion of CCRCCs harbor homozygous DNA deletions in the genomic region encompassing the *HIF1α* locus, resulting in a loss of HIF1α activity (Shen et al., 2011).

To enable cells to adapt to low-oxygen environments, HIF1α increases glycolytic flux while simultaneously suppressing glucose-dependent TCA refilling and glucose-dependent citrate biosynthesis. Moreover HIF1α facilitates the biogenesis of citrate from glutamine through reductive carboxylation to support cell proliferation in hypoxic conditions and upon TCA cycle impairment (Fendt et al., 2013; Metallo et al., 2011; Mullen et al., 2011; Wise et al., 2011). However, HIF1α represses cell autonomous proliferation, which led us to hypothesize that HIF1α could execute an additional metabolic control to override glutamine reductive carboxylation and therefore guarantee the suppression of cell proliferation. Indeed, HIF1α acts not only as a repressor of aspartate biosynthesis through glutamine oxidation but also as a simultaneous repressor of later steps in the glutamine reductive carboxylation pathway involved in cytosolic aspartate generation. In this line, HIF1α reduces the expression of key metabolic proteins involved in aspartate biogenesis, including the cytosolic and mitochondrial aspartate-producing enzymes GOT1 and GOT2. Significantly, aspartate supplementation suffices to relieve the suppression of cell proliferation upon HIF1α activation, highlighting the importance of diminished aspartate biosynthesis for the tumor-suppressive potential of HIF1α. In addition, we found that GOT1 and GOT2 are suppressed in VHL-deficient human renal carcinoma, for which HIF1α executes its tumor-suppressive potential. By identifying a role of HIF1α as a repressor of aspartate biosynthesis, we provide mechanistic insight into the molecular basis of its tumor-suppressor function through aspartate metabolic reprogramming.

RESULTS

HIF1α Reduces Aspartate Generation through Glutamine Oxidation

The intracellular molecular mechanisms that control aspartate biosynthetic pathways remain largely unknown. We questioned whether HIF1α, which acts as a suppressor of tumor cell proliferation, executes its antiproliferative effects through rewiring of aspartate metabolism. To unequivocally assess the role of HIF1α in aspartate metabolism, we restored HIF1α expression by transduction of a wild-type version of HIF1α in 786-O cells (786-O-HIF1α cells) and the corresponding control to generate 786-O-control cells as well as a mutant DNA-binding domain HIF1α (HIF1α bHLH*), lacking transcriptional activity (786-O-HIF1α bHLH* cells) (Figure 1A). Of note, to avoid an excessive

ectopic HIF1α expression, we restored HIF1α to levels similar to endogenous HIF1α in cells exposed to hypoxia (Figure S1A). We confirmed that HIF1α was active in 786-O cells by measuring the expression of carbonic anhydrase IX (CAIX), a well-recognized HIF1α-dependent gene in CCRCC (Raval et al., 2005). Accordingly, CAIX was expressed at higher levels in HIF1α-transduced cells compared with both 786-O-HIF1α bHLH* and 786-O-control cells (Figure 1A). Moreover, ectopic expression of HIF1α, but not HIF1α bHLH*, inhibited the proliferation rate of 786-O cells (Figure 1B), in line with the tumor-suppressive potential of HIF1α.

Glutamine utilization has been shown to be relevant in CCRCC biology (Fendt et al., 2013; Gameiro et al., 2013; Metallo et al., 2011; Mullen et al., 2011; Shroff et al., 2015; Wise et al., 2011). Glutamine is first converted to glutamate by the enzyme glutaminase and is subsequently converted to α-ketoglutarate (α-KG) to replenish the TCA cycle, which permits aspartate biosynthesis through glutamine oxidation (Altman et al., 2016; Birsoy et al., 2015; Buescher et al., 2015; Lane and Fan, 2015; Sullivan et al., 2015). We next assessed the levels of total glutamate, α-KG, and aspartate as well as the relative contribution of glutamine-dependent metabolism to the generation of these metabolites using $^{13}C_5$-glutamine tracer analysis (Figure 1C) in 786-O cells upon HIF1α activation. Our analysis showed an increase of total glutamate levels, while α-KG was not significantly altered in 786-O-HIF1α cells with respect to controls (Figure 1D). In sharp contrast, 786-O-HIF1α cells showed a remarkable decrease in aspartate levels compared with control cells (Figure 1D). As outlined above, we also considered aspartate generation through glutamine oxidation, in which $^{13}C_5$-glutamine is converted first to labeled M+5 glutamate and M+5 α-KG, which the latter is subsequently converted to M+4 aspartate through the TCA cycle (Figure 1C). The total content of M+5 glutamate was elevated, while M+5 α-KG generated from $^{13}C_5$-glutamine was unchanged in 786-O-HIF1α cells compared with control cells (Figure 1E). However, we observed a remarkable decrease in the total content of M+4 aspartate in 786-O cells upon HIF1α activation (Figure 1E).

We next assessed whether this rewiring of aspartate biosynthesis also occurs in other cellular settings. Loss of HIF1α has been largely investigated in VHL-deficient renal cell carcinoma cells, but deletions affecting chromosome 14q including *HIF1α* locus have been also reported in other tumor types, such as melanoma (Shen et al., 2011). Along this line, we found a spontaneously occurring subclone of melanoma cell line (UCDMel) with homozygous deletions of specific exons in the *HIF1α* locus (UCDMel-ΔH) (Figures S1B and S4G). In UCDMel-ΔH cells, we restored HIF1α activity by expressing a version of HIF1α lacking key proline hydroxylation P402 and P564 residues (HIF1α (P2)*) required for degradation in normoxia (Figure 2A). HIF1α (P2)* protein levels in UCDMel-ΔH cells were also comparable with endogenous HIF1α levels in cells exposed to hypoxia (Figure S1A). As expected, HIF1α (P2)* expression induced CAIX expression (Figure 2A) and repressed cell autonomous proliferation compared with those cells expressing the mutant DNA-binding domain HIF1α (P2)* bHLH* and the corresponding control cells (Figure 2B). Total levels of glutamate were elevated, while
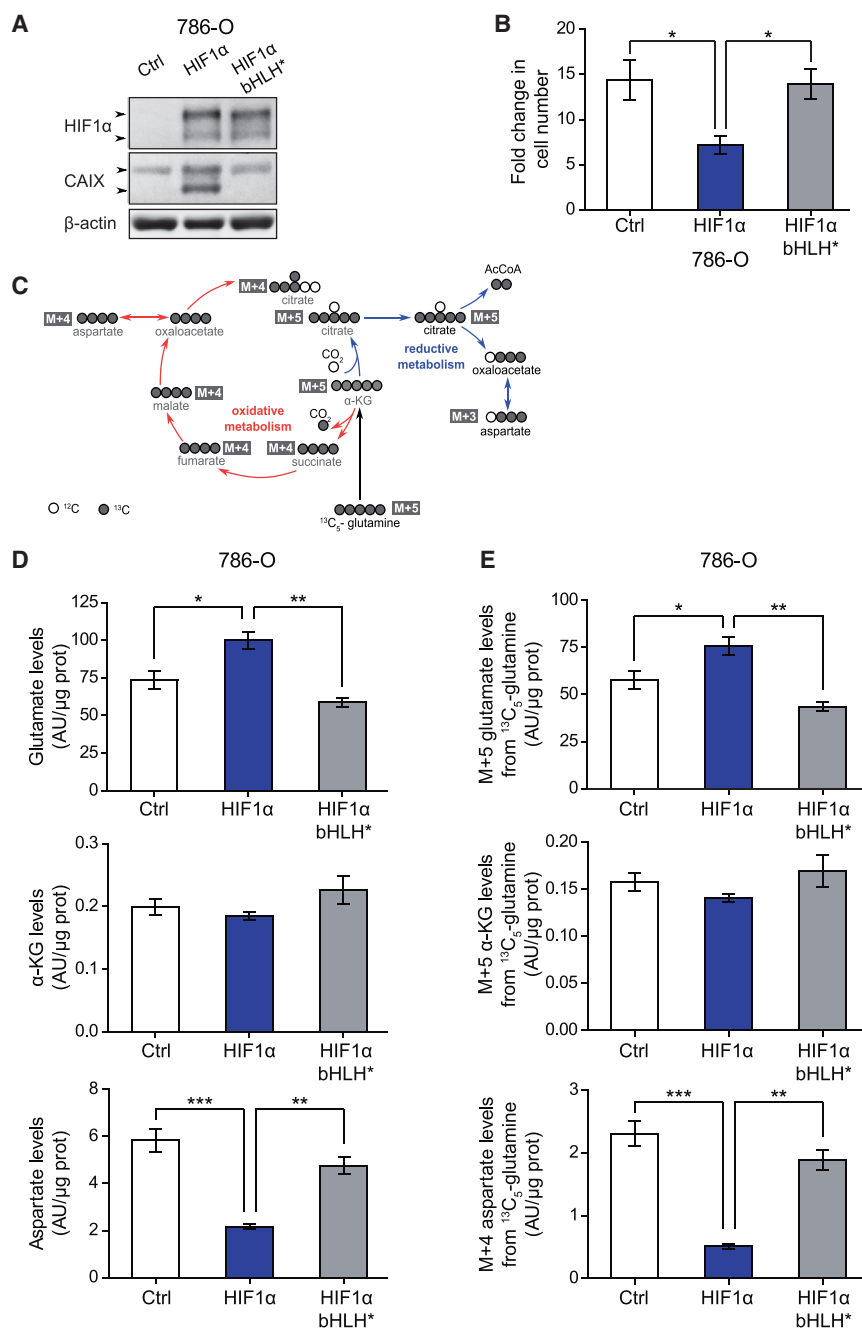
Figure 1. 786-O Cell Proliferation and Aspartate Biosynthesis through the Oxidative Pathway Are Repressed upon HIF1α Activation

(A) Representative western blot analysis of HIF1α, CAIX, and β-actin protein levels in 786-O HIF1α, HIF1α bHLH*, and control cells.

(B) Cell number fold increase of 786-O HIF1α, HIF1α bHLH*, and control cells after 96 h (n = 6).

(C) Reductive versus oxidative glutamine metabolism on the basis of a $^{13}C5$-glutamine tracer measured for α-KG, citrate, and aspartate. M+5 citrate and M+3 aspartate are indicative of reductive glutamine metabolism, whereas M+4 citrate and M+4 aspartate are indicative of oxidative glutamine metabolism. Gray circles represent ^{13}C-labeled carbons, whereas white circles represent unlabeled carbons.

(D) Total levels of glutamate, α-KG, and aspartate in 786-O HIF1α, HIF1α bHLH*, and control cells (n = 3).

(E) Absolute amount of $^{13}C_5$-glutamate (M+5), $^{13}C_5$-α-KG (M+5), and $^{13}C_4$-aspartate (M+4) derived from $^{13}C_5$-glutamine in 786-O HIF1α, HIF1α bHLH*, and control cells (n = 3).

Data are shown as mean ± SEM. Statistical analysis was performed using one-way ANOVA followed by Tukey's post hoc test. $*p < 0.05$, $**p < 0.01$, and $***p < 0.001$.

Overall, these data allow us to conclude that HIF1α represses intracellular aspartate levels and that this effect can be attributed, at least partly, to diminished glutamine-dependent aspartate biosynthesis through glutamine oxidation.

HIF1α Represses Key Mitochondrial Proteins Involved in Aspartate Biosynthesis through Glutamine Oxidation

Aspartate biosynthesis through glutamine oxidation specifically requires the activity of GOT2, which converts oxaloacetate in the mitochondrion to aspartate (Birsoy et al., 2015; Coloff et al., 2016). We thus assessed whether HIF1α represses GOT2 expression. Western blot analysis showed that GOT2 expression was lower in 786-O-HIF1α cells than in 786-O-HIF1α

total α-KG levels were modestly diminished in UCDMel-ΔH-HIF1α (P2*) cells compared with the corresponding control cells (Figure 2C). Importantly, similar to 786-O-HIF1α cells, aspartate levels were markedly lower compared with the corresponding control cells (Figure 2C). $^{13}C_5$-glutamine tracer analysis (Figure 1C) revealed that HIF1α (P2)* expression elevates total content of M+5 glutamate while M+5 α-KG was modestly diminished (Figure 2D). However, we also observed a remarkable decrease in the total content of M+4 aspartate in UCDMel-ΔH cells upon HIF1α activation (Figure 2D).

bHLH* mutant and 786-O-control cells (Figure 3A), and this was also found in UCDMel-ΔH-HIF1α (P2)* cells (Figure 3B). The expression of other aminotransferases such as phosphoserine aminotransferase (PSAT1), in which α-KG generation is coupled to non-essential amino acids (Coloff et al., 2016), was unaltered or showed an opposite trend (Figures 3A and 3B and data not shown), suggesting that the effect of HIF1α is specific to GOT2. We also considered that GOT2 requires oxaloacetate as a substrate, which is generated from malate and fumarate in the TCA cycle. In this respect, the enrichment of M+4 fumarate
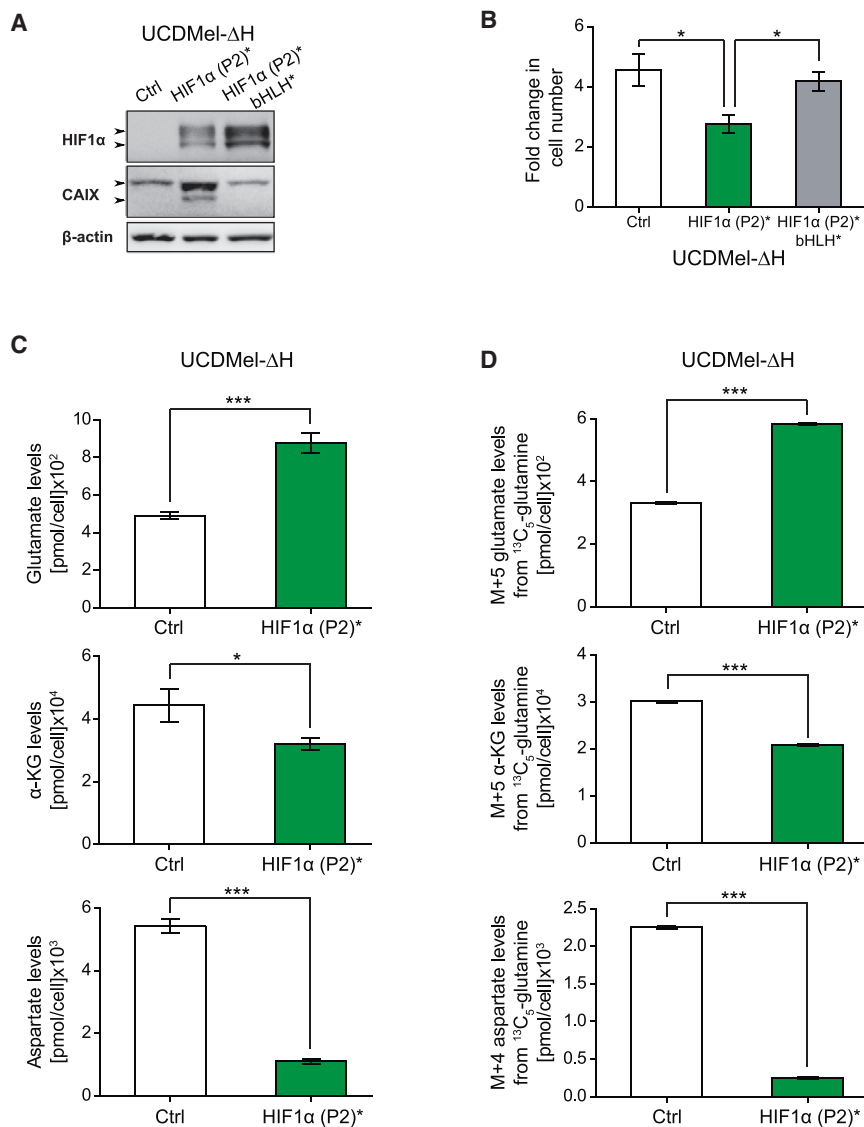
A

UCDMel-ΔH

HIF1α

CAIX

β-actin

B

UCDMel-ΔH

Figure 2. HIF1α Reduces Proliferation and Aspartate Biosynthesis through the Oxidative Pathway in UCDMel-ΔH Cells

(A) Representative western blot analysis of HIF1α, CAIX, and β-actin protein levels in UCDMel-ΔH HIF1α (P2)*, HIF1α (P2)* bHLH*, and control cells.

(B) Cell number fold increase of UCDMel-ΔH HIF1α (P2)*, HIF1α (P2)* bHLH*, and control cells after 72 h (n = 6).

(C) Total levels of glutamate, α-KG, and aspartate in UCDMel-ΔH HIF1α (P2)* and control cells (n = 3).

(D) Absolute amount of $^{13}C_5$-glutamate (M+5), $^{13}C_5$-α-KG (M+5), and $^{13}C_4$-aspartate (M+4) derived from $^{13}C_5$-glutamine in UCDMel-ΔH HIF1α (P2)* and control cells (n = 3).

Data are shown as mean ± SEM. Statistical analysis was performed using two-tailed unpaired t test when comparing two groups and one-way ANOVA followed by Tukey's post hoc test when comparing three groups. *p < 0.05 and ***p < 0.001.

C

UCDMel-ΔH

D

UCDMel-ΔH

HIF1α activity in these VHL-deficient cells can also repress GOT2 and SDH-A expression. In this line, we also found that inhibition of HIF1α in RCC4 cells by silencing of endogenous HIF1α or restoration of VHL results in an increased expression of GOT2 and SDH-A (Figures S3C and S3D).

Collectively, these data show that constitutive normoxic HIF1α activation, which acts as a tumor suppressor in VHL-deficient tumor cells, represses key proteins involved in glutamine oxidation-dependent aspartate biosynthesis such as GOT2.

HIF1α Reduces Aspartate Biosynthesis through Reductive Glutamine Metabolism

Aspartate biosynthesis can also take place in the cytosol via the GOT1 amino-

and M+4 malate from $^{13}C_5$-glutamine was also significantly decreased by HIF1α activation in 786-O and UCDMel-ΔH cells (Figures S2A and S2B). In accordance with these data, we found that HIF1α markedly repressed the expression of subunit A of succinate dehydrogenase (SDH-A), the mitochondrial complex II enzyme that converts succinate to fumarate in the TCA cycle (Figures 3A and 3B). Indeed, mitochondrial complex II activity in 786-O-HIF1α cells was significantly lower compared with control cells (Figure S2C).

Consistent with these data, we found that normoxic expression of HIF1α (P2)* at levels similar to endogenous HIF1α levels in hypoxia (Figure S1A) also repressed GOT2 and SDH-A expression in other cell lines, such as HeLa and SKOV3 (Figures S3A and S3B). In addition to VHL-deficient 786-O-like cells that lack endogenous HIF1α expression, some other VHL-deficient cells such as the widely used RCC4 cells show constitutive endogenous HIF1α expression. Therefore, we asked whether endogenous
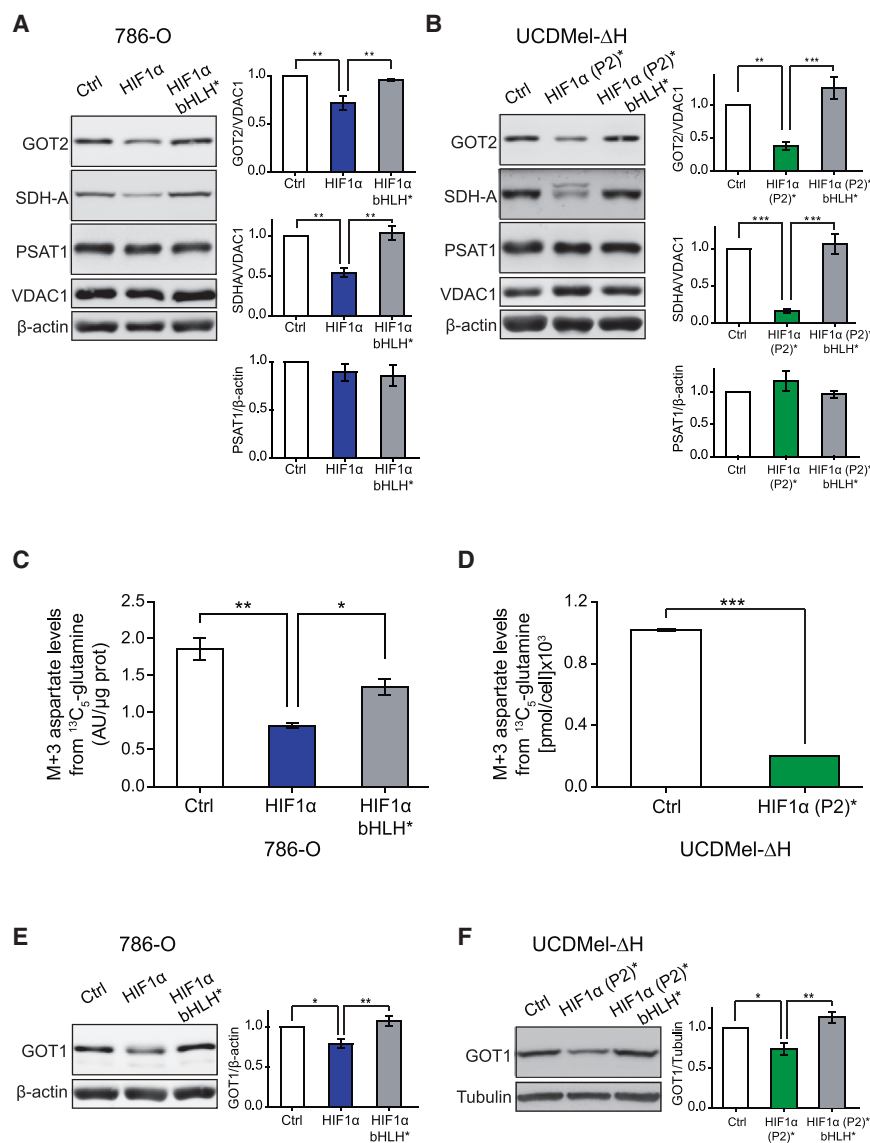
transferase isoform, which requires oxaloacetate formed from citrate generated through reductive glutamine metabolism (Birsoy et al., 2015) (Figure 1C). Previous studies have shown that citrate generation through reductive glutamine metabolism is favored upon HIF1α stabilization (Fendt et al., 2013; Gameiro et al., 2013; Metallo et al., 2011; Mullen et al., 2011; Wise et al., 2011). This shift to a reductive glutamine metabolism can be measured by the enrichment of M+5 citrate (generated through glutamine reductive carboxylation) relative to M+4 citrate (generated through glutamine oxidation). Indeed, an increased ratio of M+5 to M+4 citrate from $^{13}C_5$-glutamine is indicative of a shift from an oxidative to a reductive glutamine metabolism (Lorendeau et al., 2017) (Figure 1C). In this line, both 786-O-HIF1α and UCDMel-ΔH-HIF1α (P2)* cells showed significant increases in the enrichment of M+5 citrate relative to M+4 citrate in cells cultured in media containing $^{13}C_5$-glutamine, confirming that both cell types favor reductive

Figure 3. HIF1α Represses Key Players Involved in Biosynthesis of Mitochondrial and Cytosolic Aspartate

(A and B) Representative western blot analysis of GOT2, SDH-A, PSAT1, VDAC1, and β-actin protein levels and quantification in (A) 786-O HIF1α, HIF1α bHLH*, and control cells (n = 4) and (B) UCDMel-ΔH HIF1α (P2)*, HIF1α (P2)* bHLH*, and control cells (n = 7).

(C and D) Absolute amount of $^{13}C_3$-aspartate (M+3) derived from $^{13}C_5$-glutamine (C) in 786-O HIF1α, HIF1α bHLH*, and control cells (n = 3) and (D) in UCDMel-ΔH HIF1α (P2)* and control cells (n = 3).

(E and F) Representative western blot analysis of GOT1, tubulin, and β-actin protein levels and quantification (E) in 786-O HIF1α, HIF1α bHLH*, and control cells (n = 5) and (F) in UCDMel-ΔH HIF1α (P2)*, HIF1α (P2)* bHLH*, and control cells (n = 4).

Data are shown as mean ± SEM. Statistical analysis was performed using two-tailed unpaired t test when comparing two groups and one-way ANOVA followed by Tukey's post hoc test when comparing three groups. *$p < 0.05$, **$p < 0.01$, and ***$p < 0.001$.

carboxylation pathway for citrate generation upon HIF1α activation (Figures S2D and S2E). The reductive carboxylation pathway further converts M+5 citrate into M+3 aspartate (Figure 1C). However, our data show that the total content of M+3 aspartate from $^{13}C_5$-glutamine was markedly reduced in 786-O-HIF1α cells as well as in UCDMel-ΔH-HIF1α (P2)* cells (Figures 3C and 3D).

Moreover, these findings suggest that HIF1α can actively inhibit later steps of this reductive pathway required for cytosolic aspartate generation. Accordingly, we found that the expression of cytosolic GOT1 was decreased upon HIF1α activation in 786-O-HIF1α and UCDMel-ΔH-HIF1α (P2)* cells compared with their respective controls (Figures 3E and 3F). Suppression of GOT1 expression was also evident in HeLa and SKOV3 cells upon HIF1α (P2)* activation (Figures S4A and S4B). Furthermore, both silencing of endogenous HIF1α

in RCC4 cells as well as restoration of VHL increased GOT1 expression (Figures S4C and S4D). Finally, we explored whether HIF1α controls GOT1 and GOT2 not only when constitutively expressed under normoxia, as is observed in VHL-deficient tumor cells, but also under hypoxia. To do this, we used G55 human glioma cells, which diminished their proliferation rate and showed reduced levels of GOT1 and GOT2 under hypoxia (Figures S4E and S4F). We then silenced endogenous HIF1α to assess its role in the inhibition of cell proliferation and GOT1/2 expression in G55 cells under hypoxia. HIF1α silencing was effective, as measured by the loss of hypoxic CAIX expression (Figure S4F). Moreover, HIF1α silencing relieved the hypoxia-dependent inhibition of G55 proliferation (Figure S4E) and, importantly, counteracted the hypoxia-dependent suppression of GOT1 and GOT2 expression (Figure S4F). In agreement with these data, hypoxia did not reduce GOT1 and GOT2 expression in UCDMel-ΔH cells, which, as mentioned earlier, lack HIF1α activity and only induce the HIF2α isoform (Figure S4G).

Our data suggest that HIF1α reduces aspartate biosynthesis not only through inhibiting glutamine oxidation but also by attenuating reductive carboxylation, by repressing key players involved in these two aspartate biosynthetic pathways, such as GOT1 and GOT2. Therefore aspartate biosynthesis through reductive carboxylation upon HIF1α activation cannot compensate for the decline of aspartate generation through glutamine oxidation shown in Figures 1E and 2D.
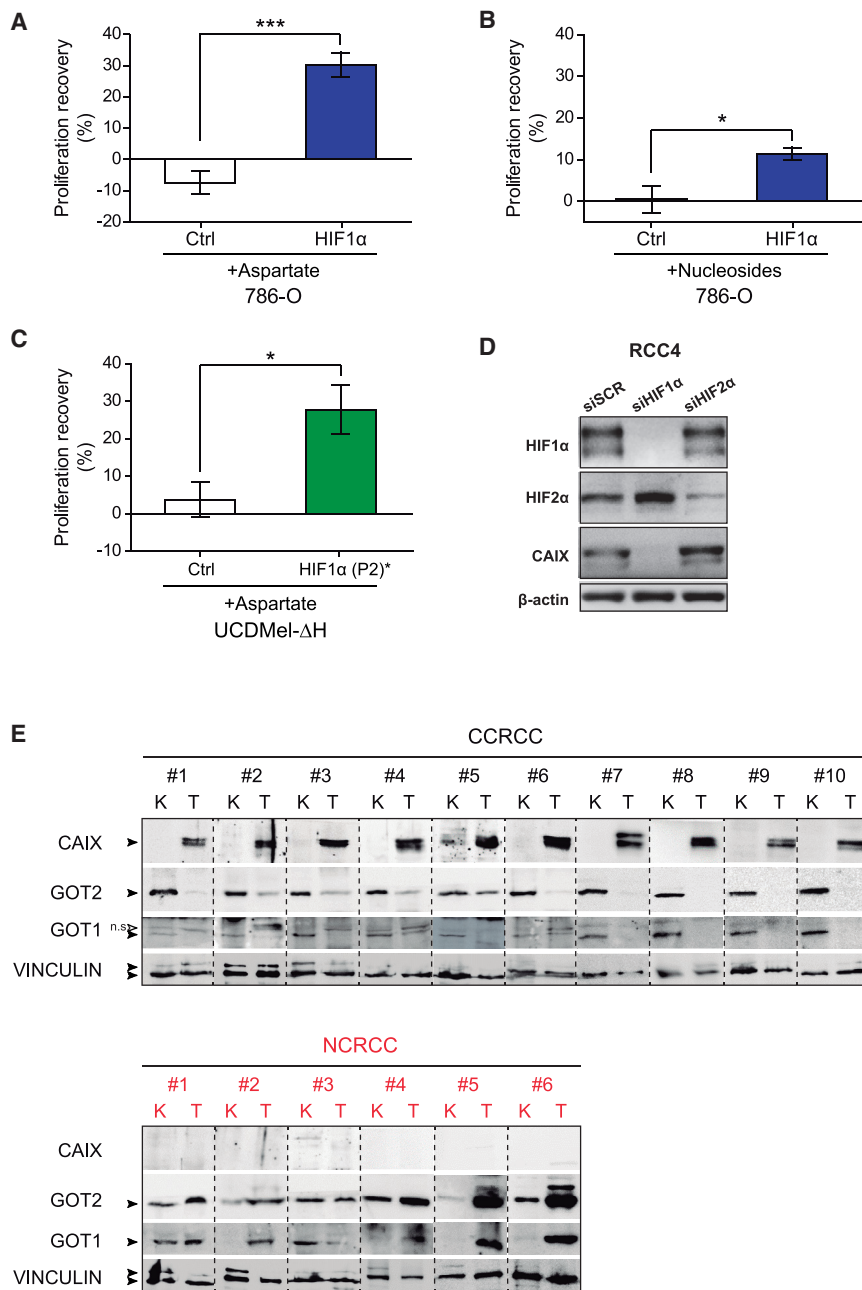
Figure 4. Effect of Aspartate Supplementation on HIF1α-Dependent Cell Proliferation Suppression and GOT1 and GOT2 Expression in Human Carcinoma Renal Samples

(A and B) Effect of (A) aspartate supplementation (50 μM) and (B) 1× nucleosides mixture supplementation on 786-O HIF1α and control cell proliferation after 96 h (n = 6).

(C) Effect of aspartate supplementation (5 mM) on UCDMel-ΔH HIF1α (P2)* and control cell proliferation after 72 h (n = 8).

(D) Representative western blot analysis of HIF1α, HIF2α, CAIX, and β-actin protein levels in transient HIF1α- and HIF2α-silenced RCC4 cells and in their corresponding control cells.

(E) Western blot analysis of CAIX, GOT2, and GOT1 expression in CCRCCs (n = 10) (top) and NCRCCs (n = 6) (bottom) together with their corresponding paired healthy adjacent kidney tissue. NCRCC samples 1, 5, and 6 were histologically classified as chromophobe; samples 2 and 4 as oncocytoma; and sample 3 as papillary renal cell carcinoma. K, normal (healthy) kidney tissue; T, tumor tissue. Black arrowheads indicate specific western blot signals, whereas the white arrowhead indicates a nonspecific signal. Vinculin was used as a loading control. n.s, non-specific.

Data are shown as mean ± SEM. Statistical analysis was performed using two-tailed unpaired t test. *p < 0.05 and ***p < 0.001.

ity to participate in the production of newly synthesized nucleotides. Consistent with this notion, we found that addition of a nucleoside mixture relieved the suppressed cell proliferation of 786-O-HIF1α cells without any significant effect on the proliferation rate of control cells (Figure 4B). This relief in cell proliferation upon supplementation with nucleosides was lower than the effect of aspartate (compare Figures 4A and 4B), but aspartate is used not only for DNA synthesis but is also required for protein synthesis. It is thus conceivable that nucleosides have a lower potential to alleviate proliferation in HIF1α-expressing cells than aspartate. Finally, we assessed whether aspartate could also counteract the antiproliferative potential of HIF1α in UCDMel-ΔH cells. Aspartate supplementation also recovered the proliferation of UCDMel-ΔH-HIF1α (P2)* cells but without any significant effect on control UCDMel-ΔH cells (Figure 4C), which further demonstrate that the ability of aspartate to relieve proliferation is specifically manifested in HIF1α-expressing cells.

Altogether, our data suggest that inhibition of aspartate biogenesis executed by HIF1α provides a metabolic basis for its prominent role in suppressing autonomous cell proliferation in different cellular settings. Indeed, HIF1α represses several key metabolic players, including GOT1 and GOT2, to ensure

Aspartate Supplementation Recovers Cell Proliferation upon HIF1α Activation

We next investigated whether intracellular aspartate decline upon HIF1α activation might be enough to explain the antiproliferative effect of HIF1α. Our earlier data showed that 786-O-HIF1α cells had significantly lower levels of aspartate than control cells (Figure 1D). Importantly, the addition of extracellular aspartate at concentration of 50 μM was sufficient to significantly stimulate the proliferation of 786-O-HIF1α cells but did not affect the proliferation of corresponding control cells (Figure 4A). The ability of aspartate to foster proliferation partially relies on its abil-

the complete inhibition of aspartate biosynthesis through the glutamine reductive carboxylation and glutamine oxidation pathways.

GOT1 and GOT2 Are Profoundly Repressed in Human VHL-Defective CCRCC

To evaluate the possible clinical implications of our data, we assessed the expression of GOT1 and GOT2 in CCRCC tumors, in which VHL activity is lost. We also included samples of non-clear renal cell carcinomas (NCRCC), which are renal carcinomas that retain VHL expression and accordingly are not characterized by constitutive HIFα activation. In total, we examined tissue samples from ten patients with CCRCC and six patients with NCRCC in parallel with adjacent healthy renal tissue from the same patient. As a specific control for HIF1α activity in these tumors, we analyzed the expression of CAIX, which is specifically driven by HIF1α, but not HIF2α, in CCRCC cell lines such as RCC4 cells (Figure 4D) (Raval et al., 2005). Compared with healthy renal tissue, all the CCRCC samples analyzed showed elevated CAIX expression, whereas no CAIX expression was detectable in any of the NCRCC samples analyzed (Figure 4E). Importantly, GOT2 expression was repressed in all CCRCC samples, and GOT1 expression was also repressed in the majority (nine of ten) of these CCRCC samples (Figure 4E). In sharp contrast to the reduced expression of GOT1 and GOT2 in CCRCC, five of six NCRCC samples showed elevated GOT1 and GOT2 expression compared with adjacent healthy renal tissue (Figure 4E). Collectively, these findings further show that human CCRCC presents a profound and simultaneous repression of GOT1 and GOT2, highlighting the relevance of the HIF1α-dependent regulation of these key players in aspartate biosynthesis in human tumors and, particularly, in VHL-deficient renal cell carcinomas. Moreover, these data underscore the clinical value of GOT1 and GOT2 repression to differentiate CCRCC and NCRCC renal cancers.

Overall, our data show that HIF1α acts as a repressor of key mitochondrial and cytoplasmic players of aspartate biosynthesis, providing a metabolic basis for the suppression of tumor cell proliferation by HIF1α in different biological settings, including VHL-deficient human carcinomas.

DISCUSSION

Aspartate has been identified as a key metabolite for cell proliferation because of its role in nucleotide synthesis (Birsoy et al., 2015; Lane and Fan, 2015; Sullivan et al., 2015). In this study, we provide evidence that HIF1α acts as a suppressor of tumor cell proliferation by controlling aspartate biosynthetic pathways. Importantly, HIF1α suppresses key players required for aspartate biosynthesis through glutamine oxidation, such as GOT2 and SDH-A. Consistent with previous studies, we found that citrate generated through glutamine reductive carboxylation is favored upon HIF1α activation (Fendt et al., 2013; Lorendeau et al., 2017; Metallo et al., 2011; Mullen et al., 2011; Wise et al., 2011) likely in an attempt to compensate for the reduced glucose-dependent citrate biosynthesis upon HIF1α activation. However, we found that HIF1α attenuates later steps in the glutamine reductive carboxylation pathway by suppressing key

players of this pathway involved in cytosolic aspartate generation, such as GOT1. It was recently shown that glutamine reductive carboxylation can contribute to aspartate generation in some VHL-deficient tumor cells (Okazaki et al., 2017). However, our data show not only that the glutamine reductive pathway does not compensate for the diminished aspartate generation through glutamine oxidation upon HIF1α activation, but that HIF1α actively limits aspartate biosynthesis through this reductive pathway involving suppression of cytosolic GOT1. Consequently, this simultaneous inhibition of oxidative and reductive pathways results in a remarkable decline in total aspartate upon HIF1α activation. In addition, it should be also considered that the simultaneous impact of HIF1α on GOT1 and GOT2 also might result into a repression on the malate-aspartate shuttle, because GOT1 also executes its well-recognized function in this shuttle by converting aspartate (generated by GOT2 in mitochondria) to oxaloacetate in the cytoplasm. Reduced glutamine oxidation metabolism can be compensated for in some tumor cells by an elevated activity of the shuttle that favors aspartate-dependent TCA cycle replenishment (Allen et al., 2016), and therefore the ability of HIF1α to suppress both players in the shuttle will ensure its function as a tumor suppressor even in cellular scenarios characterized by compensatory malate-aspartate shuttle overactivation. Importantly the inhibition of GOT1/2 expression in HIF1α-expressing cells was manifest not only in cellular in vitro settings but also in VHL-deficient human CCRCCs, which are characterized by sustained activation of HIF1α but not in NCRCCs which lack constitutive HIF1α activation. Thus, GOT1 and GOT2 repression represents a specific metabolic feature of CCRCC. These findings not only support the notion that the repressive HIF1α-GOT1/2 pathway is operative in vivo in human tumors but also underscore the clinical value of our data to differentiate between CCRCC and NCRCC renal cancers. Finally it should also be stated that a recent metabolomic study of CCRCC found that these tumors have low aspartate levels (Hakimi et al., 2016), and in vivo studies showed glutamine metabolism to have a dominant role in sustaining CCRCC growth (Shroff et al., 2015). It is therefore plausible that HIF1α counteracts glutamine-dependent metabolic pathways in order to act as a tumor suppressor in CCRCC.

Notably, the relevance of aspartate insufficiency imposed by HIF1α tumor-suppressive activity was demonstrated by the fact that aspartate supplementation relieved HIF1α-dependent suppression of cell proliferation. Cancer cells have limited ability to uptake aspartate compared with other metabolites (Birsoy et al., 2015; Garcia-Bermudez et al., 2018; Sullivan et al., 2015, 2018). In this line, previous studies have shown that aspartate is required at concentrations of 5–20 mM to restore proliferation of cells lacking mitochondrial activity (Birsoy et al., 2015; Sullivan et al., 2015). However, some tumor cell types show basal expression of the high-affinity aspartate transporter SLC1A3 to import aspartate, and therefore lower doses are sufficient to restore proliferation of these cells when mitochondrial activity is compromised (Garcia-Bermudez et al., 2018). In this study we found that aspartate doses required to increase proliferation in 786-O-HIF1α cells are lower than in UCDMel-ΔH cells, possibly related to the higher expression of SLC1A3 in 786-O than in UCDMel-ΔH cells (data not shown). In agreement with

our data, it was shown that hypoxia reduces intracellular aspartate levels and that hypoxia-dependent suppression of cell proliferation can be recovered by aspartate supplementation (Garcia-Bermudez et al., 2018; Sullivan et al., 2018). However, it should be highlighted that these studies considered that oxygen insufficiency might restrict aspartate biosynthesis through a direct impairment of electron transport chain function, limiting the generation of electron acceptors required for aspartate synthesis. Our data show that the hypoxia-dependent suppression of aspartate metabolism is not necessarily a consequence of a direct impact on mitochondrial activity but importantly also requires the HIF1α oxygen-sensing pathway that promotes multiple actions that compromise aspartate biosynthesis. Therefore these data show that HIF1α pathway couples cellular oxygen supply and aspartate biosynthesis.

In summary, our study identifies HIF1α as an inhibitor of aspartate biogenesis by repressing glutamine oxidation and reductive carboxylation pathways, effects that include the suppression of several metabolic players involved in aspartate production, such as GOT1 and GOT2. This pathway provides a molecular basis for the effect of HIF1α in suppressing tumor cell proliferation that is operative in several biological settings, including human CCRCC, for which HIF1α acts as a tumor suppressor.

STAR★METHODS

Detailed methods are provided in the online version of this paper and include the following:

- KEY RESOURCES TABLE
- CONTACT FOR REAGENT AND RESOURCE SHARING
- EXPERIMENTAL MODEL AND SUBJECT DETAILS
  - Cell cultures
  - Clinical material
- METHOD DETAILS
  - DNA constructs
  - Viral infection
  - siRNA-mediated gene silencing
  - Western blots and antibodies
  - Cell proliferation analysis
  - $^{13}C_5$-glutamine tracer analysis
  - Mitochondrial membranes isolation and SDH activity
  - Protein expression analysis of clinical material
  - Massive parallel sequencing
- QUANTIFICATION AND STATISTICAL ANALYSIS

SUPPLEMENTAL INFORMATION

Supplemental Information can be found with this article online at https://doi.org/10.1016/j.celrep.2019.01.106.

AUTHOR CONTRIBUTIONS

F.M.-R. and A.A.U. conducted most of the experiments. F.M.-R., A.A.U., S.-M.F., K.D.B., and J.A. were involved in the design of the experiments, data analysis, and writing the manuscript. C.M.-C., G.T., Q.O.Y.L., E. Fuertes, E.E., and K.D.B. helped with proliferation experiments. A.E., M.T.-C., D.T., and E. Fuertes helped with western blot and RNA analysis. A.B. and E. Fraga helped with aspartate supplementation experiments. D.L. and G.R. performed the $^{13}C_5$-glutamine dynamic tracer experiments and total intracellular metabolite level measurements. N.B.-S. and T.A. performed the analysis in hypoxia-exposed G55 cells. O.R., A.S.S.-S., J.M.G.-B., M.O.M., and R.S.P. helped with collection and western blot analysis of human samples of renal cell carcinoma. P.H.-A. and A.M.-R. helped with mitochondrial complex II activity measurements. B.P. helped with identification of *HIF1α* locus deletions in UCD-Mel-ΔH cells.

DECLARATION OF INTERESTS

The authors declare no competing interests.

REFERENCES

Allen, E.L., Ulanet, D.B., Pirman, D., Mahoney, C.E., Coco, J., Si, Y., Chen, Y., Huang, L., Ren, J., Choe, S., et al. (2016). Differential aspartate usage identifies a subset of cancer cells particularly dependent on OGDH. Cell Rep. *17*, 876–890.

Altman, B.J., Stine, Z.E., and Dang, C.V. (2016). From Krebs to clinic: glutamine metabolism to cancer therapy. Nat. Rev. Cancer *16*, 619–634.

Birsoy, K., Wang, T., Chen, W.W., Freinkman, E., Abu-Remaileh, M., and Sabatini, D.M. (2015). An essential role of the mitochondrial electron transport chain in cell proliferation is to enable aspartate synthesis. Cell *162*, 540–551.

Buescher, J.M., Antoniewicz, M.R., Boros, L.G., Burgess, S.C., Brunengraber, H., Clish, C.B., DeBerardinis, R.J., Feron, O., Frezza, C., Ghesquiere, B., et al. (2015). A roadmap for interpreting (13)C metabolite labeling patterns from cells. Curr. Opin. Biotechnol. *34*, 189–201.

Carmeliet, P., Dor, Y., Herbert, J.M., Fukumura, D., Brusselmans, K., Dewerchin, M., Neeman, M., Bono, F., Abramovitch, R., Maxwell, P., et al. (1998). Role of HIF-1alpha in hypoxia-mediated apoptosis, cell proliferation and tumour angiogenesis. Nature *394*, 485–490.

Coloff, J.L., Murphy, J.P., Braun, C.R., Harris, I.S., Shelton, L.M., Kami, K., Gygi, S.P., Selfors, L.M., and Brugge, J.S. (2016). Differential glutamate metabolism in proliferating and quiescent mammary epithelial cells. Cell Metab. *23*, 867–880.

Epstein, A.C., Gleadle, J.M., McNeill, L.A., Hewitson, K.S., O'Rourke, J., Mole, D.R., Mukherji, M., Metzen, E., Wilson, M.I., Dhanda, A., et al. (2001).

C. elegans EGL-9 and mammalian homologs define a family of dioxygenases that regulate HIF by prolyl hydroxylation. Cell *107*, 43–54.

Fendt, S.M., Bell, E.L., Keibler, M.A., Olenchock, B.A., Mayers, J.R., Wasylenko, T.M., Vokes, N.I., Guarente, L., Vander Heiden, M.G., and Stephanopoulos, G. (2013). Reductive glutamine metabolism is a function of the α-ketoglutarate to citrate ratio in cells. Nat. Commun. *4*, 2236.

Fernandez, C.A., Des Rosiers, C., Previs, S.F., David, F., and Brunengraber, H. (1996). Correction of 13C mass isotopomer distributions for natural stable isotope abundance. J. Mass Spectrom. *31*, 255–262.

Gameiro, P.A., Yang, J., Metelo, A.M., Pérez-Carro, R., Baker, R., Wang, Z., Arreola, A., Rathmell, W.K., Olumi, A., López-Larrubia, P., et al. (2013). In vivo HIF-mediated reductive carboxylation is regulated by citrate levels and sensitizes VHL-deficient cells to glutamine deprivation. Cell Metab. *17*, 372–385.

Garcia-Bermudez, J., Baudrier, L., La, K., Zhu, X.G., Fidelin, J., Sviderskiy, V.O., Papagiannakopoulos, T., Molina, H., Snuderl, M., Lewis, C.A., et al. (2018). Aspartate is a limiting metabolite for cancer cell proliferation under hypoxia and in tumours. Nat. Cell Biol. *20*, 775–781.

Gordan, J.D., Bertout, J.A., Hu, C.J., Diehl, J.A., and Simon, M.C. (2007). HIF-2alpha promotes hypoxic cell proliferation by enhancing c-myc transcriptional activity. Cancer Cell *11*, 335–347.

Hakimi, A.A., Reznik, E., Lee, C.H., Creighton, C.J., Brannon, A.R., Luna, A., Aksoy, B.A., Liu, E.M., Shen, R., Lee, W., et al. (2016). An integrated metabolic atlas of clear cell renal cell carcinoma. Cancer Cell *29*, 104–116.

Hubbi, M.E., Kshitiz, Gilkes, D.M., Rey, S., Wong, C.C., Luo, W., Kim, D.H., Dang, C.V., Levchenko, A., and Semenza, G.L. (2013). A nontranscriptional role for HIF-1α as a direct inhibitor of DNA replication. Sci. Signal. *6*, ra10.

Ivan, M., Kondo, K., Yang, H., Kim, W., Valiando, J., Ohh, M., Salic, A., Asara, J.M., Lane, W.S., and Kaelin, W.G., Jr. (2001). HIFalpha targeted for VHL-mediated destruction by proline hydroxylation: implications for O2 sensing. Science *292*, 464–468.

Jaakkola, P., Mole, D.R., Tian, Y.M., Wilson, M.I., Gielbert, J., Gaskell, S.J., von Kriegsheim, A., Hebestreit, H.F., Mukherji, M., Schofield, C.J., et al. (2001). Targeting of HIF-alpha to the von Hippel-Lindau ubiquitylation complex by O2-regulated prolyl hydroxylation. Science *292*, 468–472.

Kaelin, W.G., Jr. (2008). The von Hippel-Lindau tumour suppressor protein: O2 sensing and cancer. Nat. Rev. Cancer *8*, 865–873.

Kondo, K., Kim, W.Y., Lechpammer, M., and Kaelin, W.G., Jr. (2003). Inhibition of HIF2alpha is sufficient to suppress pVHL-defective tumor growth. PLoS Biol. *1*, E83.

Labrousse-Arias, D., Castillo-González, R., Rogers, N.M., Torres-Capelli, M., Barreira, B., Aragonés, J., Cogolludo, Á., Isenberg, J.S., and Calzada, M.J. (2016). HIF-2α-mediated induction of pulmonary thrombospondin-1 contributes to hypoxia-driven vascular remodelling and vasoconstriction. Cardiovasc. Res. *109*, 115–130.

Lane, A.N., and Fan, T.W. (2015). Regulation of mammalian nucleotide metabolism and biosynthesis. Nucleic Acids Res. *43*, 2466–2485.

Lapuente-Brun, E., Moreno-Loshuertos, R., Acín-Pérez, R., Latorre-Pellicer, A., Colás, C., Balsa, E., Perales-Clemente, E., Quirós, P.M., Calvo, E., Rodríguez-Hernández, M.A., et al. (2013). Supercomplex assembly determines electron flux in the mitochondrial electron transport chain. Science *340*, 1567–1570.

Lorendeau, D., Rinaldi, G., Boon, R., Spincemaille, P., Metzger, K., Jager, C., Christen, S., Dong, X., Kuenen, S., Voordeckers, K., et al. (2017). Dual loss of

succinate dehydrogenase (SDH) and complex I activity is necessary to recapitulate the metabolic phenotype of SDH mutant tumors. Metab. Eng. *43*, 187–197.

Mayers, J.R., and Vander Heiden, M.G. (2015). Famine versus feast: understanding the metabolism of tumors in vivo. Trends Biochem. Sci. *40*, 130–140.

Metallo, C.M., Gameiro, P.A., Bell, E.L., Mattaini, K.R., Yang, J., Hiller, K., Jewell, C.M., Johnson, Z.R., Irvine, D.J., Guarente, L., et al. (2011). Reductive glutamine metabolism by IDH1 mediates lipogenesis under hypoxia. Nature *481*, 380–384.

Mullen, A.R., Wheaton, W.W., Jin, E.S., Chen, P.H., Sullivan, L.B., Cheng, T., Yang, Y., Linehan, W.M., Chandel, N.S., and DeBerardinis, R.J. (2011). Reductive carboxylation supports growth in tumour cells with defective mitochondria. Nature *481*, 385–388.

Okazaki, A., Gameiro, P.A., Christodoulou, D., Laviollette, L., Schneider, M., Chaves, F., Stemmer-Rachamimov, A., Yazinski, S.A., Lee, R., Stephanopoulos, G., et al. (2017). Glutaminase and poly(ADP-ribose) polymerase inhibitors suppress pyrimidine synthesis and VHL-deficient renal cancers. J. Clin. Invest. *127*, 1631–1645.

Raval, R.R., Lau, K.W., Tran, M.G., Sowter, H.M., Mandriota, S.J., Li, J.L., Pugh, C.W., Maxwell, P.H., Harris, A.L., and Ratcliffe, P.J. (2005). Contrasting properties of hypoxia-inducible factor 1 (HIF-1) and HIF-2 in von Hippel-Lindau-associated renal cell carcinoma. Mol. Cell. Biol. *25*, 5675–5686.

Shen, C., Beroukhim, R., Schumacher, S.E., Zhou, J., Chang, M., Signoretti, S., and Kaelin, W.G., Jr. (2011). Genetic and functional studies implicate HIF1α as a 14q kidney cancer suppressor gene. Cancer Discov. *1*, 222–235.

Shroff, E.H., Eberlin, L.S., Dang, V.M., Gouw, A.M., Gabay, M., Adam, S.J., Bellovin, D.I., Tran, P.T., Philbrick, W.M., Garcia-Ocana, A., et al. (2015). MYC oncogene overexpression drives renal cell carcinoma in a mouse model through glutamine metabolism. Proc. Natl. Acad. Sci. U S A *112*, 6539–6544.

Sullivan, L.B., Gui, D.Y., Hosios, A.M., Bush, L.N., Freinkman, E., and Vander Heiden, M.G. (2015). Supporting aspartate biosynthesis is an essential function of respiration in proliferating cells. Cell *162*, 552–563.

Sullivan, L.B., Luengo, A., Danai, L.V., Bush, L.N., Diehl, F.F., Hosios, A.M., Lau, A.N., Elmiligy, S., Malstrom, S., Lewis, C.A., and Vander Heiden, M.G. (2018). Aspartate is an endogenous metabolic limitation for tumour growth. Nat. Cell Biol. *20*, 782–788.

Wang, G.L., Jiang, B.H., Rue, E.A., and Semenza, G.L. (1995). Hypoxia-inducible factor 1 is a basic-helix-loop-helix-PAS heterodimer regulated by cellular O2 tension. Proc. Natl. Acad. Sci. U S A *92*, 5510–5514.

Wise, D.R., Ward, P.S., Shay, J.E., Cross, J.R., Gruber, J.J., Sachdeva, U.M., Platt, J.M., DeMatteo, R.G., Simon, M.C., and Thompson, C.B. (2011). Hypoxia promotes isocitrate dehydrogenase-dependent carboxylation of α-ketoglutarate to citrate to support cell growth and viability. Proc. Natl. Acad. Sci. U S A *108*, 19611–19616.

Yan, Q., Bartz, S., Mao, M., Li, L., and Kaelin, W.G., Jr. (2007). The hypoxia-inducible factor 2alpha N-terminal and C-terminal transactivation domains cooperate to promote renal tumorigenesis in vivo. Mol. Cell. Biol. *27*, 2092–2102.

Young, J.D., Walther, J.L., Antoniewicz, M.R., Yoo, H., and Stephanopoulos, G. (2008). An elementary metabolite unit (EMU) based method of isotopically nonstationary flux analysis. Biotechnol. Bioeng. *99*, 686–699.

STAR★METHODS

KEY RESOURCES TABLE

REAGENT or RESOURCE	SOURCE	IDENTIFIER
Antibodies		
Mouse monoclonal anti-HIF1α	BD Transduction Lab.	Cat#610959; RRID: AB_398272
Rabbit polyclonal anti-HIF2α	Abcam	Cat#ab199; RRID: AB_302739
Mouse monoclonal anti-CAIX	Santa Cruz Biotech.	Cat#sc-365900; RRID: AB_10846466
Mouse monoclonal anti-Tubulin	Sigma Aldrich	Cat#T6199; RRID: AB_477583
Monoclonal anti-β-actin−peroxidase	Sigma Aldrich	Cat#A3854; RRID: AB_262011
Mouse monoclonal anti-Vinculin	Sigma Aldrich	Cat#V9264; RRID: AB_10603627
Rabbit polyclonal anti-VDAC1/Porin	Abcam	Cat#ab15895; RRID: AB_2214787
Rabbit polyclonal anti-GOT1	ProteinTech	Cat#14886-1-AP; RRID: AB_2113630
Rabbit polyclonal anti-GOT1	Novus Biologicals	Cat#NBP1-54778, RRID: AB_11006805
Rabbit polyclonal anti-GOT2	Sigma Aldrich	Cat#HPA018139; RRID: AB_1849903
Rabbit polyclonal anti-PSAT1	ThermoFisher	Cat#PA5-22124; RRID: AB_11153526
Rabbit monoclonal anti-SDH-A	Abcam	Cat#ab137040
Biological Samples		
Human renal carcinoma samples	Urology Department of the University Complex of Albacete	N/A
Healthy human renal samples	Urology Department of the University Complex of Albacete	N/A
Chemicals, Peptides, and Recombinant Proteins		
Polybrene	Santa Cruz Biotech.	Cat#sc-134220
$^{13}C_5$-glutamine	Sigma Aldrich	Cat#605166
L-aspartic acid	Sigma Aldrich	Cat#A7219
EmbryoMax® Nucleosides (100X)	Merck	Cat#ES-008-D
Phosphatase inhibitors	Sigma Aldrich	Cat#P5726
Protease inhibitors	Sigma Aldrich	Cat#P8340
Experimental Models: Cell Lines		
HEK293T	Provided by Dr. María J. Calzada	N/A
786-O	Provided by Dr. María J. Calzada	N/A
UCDMel-ΔH	This paper	N/A
HeLa	Provided by Dr. María J. Calzada	N/A
SKOV3	Provided by Dr. María J. Calzada	N/A
RCC4	Provided by Dr. María J. Calzada	N/A
G55	Provided by Dr. Till Acker	N/A
Oligonucleotides		
Control siRNA	Santa Cruz Biotech.	Cat#sc-37007
HIF1α siRNA	Santa Cruz Biotech.	Cat#sc-35561
HIF2α siRNA	Dharmacon	Cat#L-004814-00-0005
Recombinant DNA		
pLVX-TetOne-Puro-Luc	Takara	Cat#631849
pLVX-TetOne-HIF1α	This paper	N/A
pLVX-TetOne-HIF1α bHLH*	This paper	N/A
pRV	Labrousse-Arias et al., 2016	N/A
pRV-HIF1α (P2)*	Labrousse-Arias et al., 2016	N/A
pRV-HIF1α (P2)* bHLH*	Labrousse-Arias et al., 2016	N/A

Continued

REAGENT or RESOURCE	SOURCE	IDENTIFIER
pLVX	Takara	Cat#632159
pLVX-VHL	This paper	N/A
pGIPZ-shSCR	Dharmacon	Cat# RHS4346
pGIPZ-shHIF1α	Dharmacon	Cat# RHS4531-EG3091
Other		
Lipofectamine 2000 Transfection Reagent	Invitrogen	Cat#11668019
Dialyzed fetal bovine serum	Sigma Aldrich	Cat#F0392

CONTACT FOR REAGENT AND RESOURCE SHARING

Further information and requests for reagents may be directed to and will be fulfilled by the Lead Contact, Julián Aragonés (jaragones.hlpr@salud.madrid.org).

EXPERIMENTAL MODEL AND SUBJECT DETAILS

Cell cultures

The HEK293T, 786-O, UCDMel-ΔH, HeLa, SKOV3, RCC4 and G55 cell lines were maintained in Dulbecco's modified Eagle's medium (DMEM, HyClone, GE HealthCare) with the addition of 100 units/ml penicillin, 100 μg/ml streptomycin, 20 mM HEPES and 10% fetal bovine serum (FBS, Cultek). G55 cells were cultured in DMEM (ThermoFisher Scientific) supplemented with 10% fetal bovine serum (FBS, Merck). Cells were maintained at 37°C in an atmosphere of 5% CO_2/95% air (normoxic conditions). To induce hypoxia, the cell culture dishes were placed at 0.5%–1% O_2 conditions. For supplementation assays, we used DMEM containing 10% dialyzed FBS (10,000 Mwt cut-off; F0392, Sigma), which was then supplemented with aspartate (A7219, Sigma-Aldrich) or a mixture of nucleosides (ES-008-D, Merck) when necessary.

Clinical material

Fresh human samples were obtained under the supervision of the pathologist and the local ethical committee from patients diagnosed and treated surgically at the Urology Department of the University Complex of Albacete, and without interfering with their histological evaluation. All cases were reviewed and diagnosed according to the criteria of the World Health Organization classification. Sample numbers are detailed in Figure 4 and its figure legend.

Patient gender and age (years)

	#	Sex	Age (years)
CCRCC	1	Male	82
	2	Male	77
	3	Male	68
	4	Female	75
	5	Female	78
	6	Male	49
	7	Male	76
	8	Male	43
	9	Male	47
	10	Male	40
NCRCC	1	Female	52
	2	Male	53
	3	Male	59
	4	Male	73
	5	Female	42
	6	Female	63

METHOD DETAILS

DNA constructs

To generate 786-O cells stably expressing HIF1α, we used a lentiviral vector pLVX-TetOne-Puro (Takara) harboring a wild-type version of HIF1α, as well as pLVX-TetOne-Puro-Luc as its corresponding control vector. As an additional control, we utilized a lentiviral vector encoding HIF1α bHLH*, a version of HIF1α into which we introduced a four amino acid substitution within the basic helix–loop–helix (bHLH) domain that impedes its transcriptional activity (similar to the four amino acid substitution previously introduced into HIF2α (P2)* (Kondo et al., 2003)). Cells were transduced and then selected with 1 μg/ml puromycin (to obtain resistant polyclonal cell pools) and treated with 1 μg/ml doxycycline (to induce the vector expression).

To generate UCDMel-ΔH, HeLa and SKOV3 cell lines stably expressing HIF1α, we used a retroviral vector pRV encoding a mutated version of HIF1α at positions P402 and P564 (HIF1α (P2)*), which therefore lacks critical proline residues and is therefore not recognized by VHL. Accordingly, this construct is constitutively active in normoxic conditions irrespective of the oxygen tension (Yan et al., 2007). In addition to the empty vector pRV, as an additional control, we utilized a retroviral vector encoding HIF1α (P2)* bHLH*, a version of HIF1α (P2)* into which we introduced a four amino acid substitution within the basic helix–loop–helix (bHLH) domain that impedes its transcriptional activity (similar to the four amino acid substitution previously introduced into HIF2α (P2)* (Kondo et al., 2003)).

Lentiviral pLVX-VHL and pGIPZ-shHIF1α vectors and their corresponding pLVX and pGIPZ-shSCR (Dharmacon) control vectors were used to generate stable transfectants of RCC4 cells. Cells were transduced and then selected with 1 μg/ml puromycin to obtain resistant polyclonal cell pools.

Viral infection

For retroviral infection, HEK293T cells seeded in p60 plates were transfected with 4 μg of each retroviral vector and 4 μg of the pCL-Ampho Retrovirus Packaging Vector (Imgenex) using Lipofectamine 2000 (Invitrogen). Cell culture supernatants were harvested 24 hours after transfection, filtered through a 0.45 μm filter, diluted (1:2) with fresh medium containing 8 μg/ml polybrene (final concentration) and added to the corresponding cells. This step was repeated on the next 2 days. For lentiviral infection, HEK293T cells seeded in p60 plates were transfected with 1.3 μg of pLP1, 0.9 μg of pLP2, 1.1 μg of VSVg and 3.3 μg of each lentiviral vector, following the same protocol as for retroviral infection.

siRNA-mediated gene silencing

The siRNA experiments were carried out using HIF1α siRNA (sc-35561, Santa Cruz Biotechnology), HIF2α siRNA (L-004814-00-0005, Dharmacon) and control siRNA (sc-37007, Santa Cruz Biotechnology). RCC4 cells seeded in p60 plates were transfected with 60 nM of the corresponding siRNA using Lipofectamine 2000 (Invitrogen). After 72 hours post-transfection, cells were collected and stored at −20°C until processing for western blot analysis.

Western blots and antibodies

Cells were lysed in Laemmli buffer. Proteins were resolved in 8% or 10% SDS-polyacrylamide gels and transferred to 0.45 μm nitrocellulose membranes. The membranes were blocked and probed with antibodies against: HIF2α (ab199, Abcam); HIF1α (610959,BD Transduction Laboratories); tubulin (T6199, Sigma); β-actin (A3854, Sigma); VDAC1/Porin (ab15895, Abcam); GOT2 (HPA018139, Sigma Aldrich); GOT1 (14886-1-AP, ProteinTech); PSAT1 (PA5-22124, Thermo Fisher); SDH-A (ab137040, Abcam); and CAIX (sc-365900, Santa Cruz Biotechnology). Immunoreactivity was detected by enhanced chemiluminiscence (Clarity, BioRad; and SuperSignal West Femto Maximum Sensitivity Substrate, Thermo Scientific) and visualized on a digital luminescent image analyzer (Image Quant LAS4000 Mini; GE Healthcare).

Cell proliferation analysis

For cell proliferation assays, 40,000 UCDMel-ΔH cells or 20,000 786-O cells were seeded per well in 6-well plates. After 72 hours for UCDMel-ΔH cells or 96 hours for 786-O cells, they were trypsinized and collected in the medium and live cells per well were counted manually with Neubauer Chamber.

For cell proliferation recovery assays with UCDMel-ΔH and 786-O cells, after 6 hours from seeding them, the medium was changed to medium supplemented with dialyzed FBS and with or without aspartate (5 mM or 50 μM, respectively) or a mixture of nucleosides (1x working concentration). Then cells were grown for a further 72 or 96 hours and collected and counted as described before. Data were expressed as the percentage of proliferation recovery relative to equivalent cells cultured in non-supplemented medium.

G55 (30,000 cells) were seeded per well in 12-well plate. After 6 days later, cells were trypsinized and collected in the medium, and live cells per well were counted by CASY (OMNI Life Science).

$^{13}C_5$-glutamine tracer analysis

The $^{13}C_5$-glutamine tracer (Sigma-Aldrich) was added to cells grown to confluency. The medium was changed for unlabeled medium 1 hour before adding the $^{13}C_5$-glutamine medium. Cells were exposed to $^{13}C_5$-glutamine in medium containing dialyzed FBS for 4 hours, after which time the metabolites were extracted. Control cells were maintained in unlabeled media in parallel to determine

the cell numbers. Metabolites for mass spectrometry (MS) analysis were prepared by quenching the cells in liquid nitrogen and then performing a cold, two-phase, methanol-water-chloroform extraction (Lorendeau et al., 2017), followed by centrifugation at 4°C to achieve phase separation. The methanol-water phase containing polar metabolites was separated and dried in a vacuum concentrator, and then stored at −80°C. Polar metabolites were derivatized for 90 minutes at 37°C with 7.5 μL of 20 mg ml^{-1} methoxyamine in pyridine and subsequently, for 60 minutes at 60°C with 15 μL of N-(tert-butyldimethylsilyl)-N-methyltrifluoroacetamide, with 1% tert-butyldimethylchlorosilane (Lorendeau et al., 2017). Isotopomer distributions and metabolite concentrations were measured on a 7890A GC system (Agilent Technologies) combined with a 5975C Inert MS system (Agilent Technologies). The samples (1 μl) were injected onto a DB35MS column in splitless mode using an inlet temperature of 270°C. The carrier gas was helium with a flow rate of 1 mL min^{-1}. Upon injection, the GC oven was held at 100°C for 3 minutes and then ramped to 300°C with a gradient of 2.5°C min^{-1}, followed by a 5 minute after run at 320°C. The MS system was operated under electron impact ionization at 70 eV and a mass range of 100–650 amu was scanned. Isotopomer distributions were extracted from the raw ion chromatograms using a custom MATLAB M-file that applies consistent integration boundaries and baseline correction to each ion (Young et al., 2008). In addition, we corrected for naturally occurring isotopes (Fernandez et al., 1996) and for potential metabolite contamination using a blank extraction. All labeling fractions were transformed to a natural abundance corrected mass distribution vector (MDV: (Buescher et al., 2015)). Negative values were considered as zero. Each metabolite was measured in n = 3 biological replicates. The aforementioned script also provides information about the total abundance of each metabolite in arbitrary units. Specifically, areas under the metabolite peak were normalized the internal standards norvaline or glutarate, as well as cell number or protein content. Conversion to absolute abundance in pmol was based on standard curves of known metabolite concentration.

Mitochondrial membranes isolation and SDH activity

Mitochondria were isolated from 786-O HIF1α and HIF1α bHLH* cells as well as from their corresponding 786-O control cells following a protocol adapted for cell culture (Lapuente-Brun et al., 2013). Briefly, after resuspending cells with a sucrose buffer in a glass Elvehjem potter, homogenization was performed by up and down strokes using a motor-driven Teflon pestle. Successive homogenization-centrifugation steps yielded the mitochondria-containing fraction. Mitochondrial membranes were obtained after freezing isolated mitochondria.

Succinate dehydrogenase (complex II) activity was measured by recording changes in absorbance at 600 nm in a buffer (25 mM K$_2$HPO$_4$, 5 mM MgCl$_2$, 3 mM KCN and 2.5 mg/ml BSA, pH 7.2) containing 50-100 μg mitochondrial membranes, 10 mM succinate, 5 μM 2,6-dichlorophenol-indophenol (DCPIP), 2 μg/ml antimycin A, 5 μM rotenone and 130 μM CoQ$_1$.

Protein expression analysis of clinical material

Kidney tumor and adjacent healthy tissue fresh samples were obtained in the surgery room and embedded in Optimal Cutting Temperature (OCT) medium introducing in isopentane at −80°C. Samples were maintained at −80°C until the sample was processed. Samples were cutted in pieces of 25 μm with a cryostat microtome. Protein extraction was realized from 15 sections. First, 1 mL of water was added to the OCT embedded samples, and incubated 15 minutes on ice. Samples were centrifuged in a microcentrifuge 2 minutes at 10,000 rpm at 4°C. Lysis buffer (100 mM HEPES, pH 7.5; 50 mM NaCl; 0.1% Triton X-100; 5 mM EDTA; 0.125 M EGTA, protease (P8340, Sigma) and phosphatase inhibitors cocktail (P5726, Sigma)) were added to the pellet and tissue was disgregated with a plunger. Afterward, samples were shaken at 4°C for 30 minutes, and followed up by 15 minutes centrifugation at 4°C at 12000 rpm. Supernatant containing the protein was collected.

Indicated amounts of protein were loaded onto 10% SDS-PAGE, transferred to PVDF filters and blotted against different proteins using antibodies against GOT2 (HPA018139, Sigma Aldrich); GOT1 (NBP1-54778, Novus); CAIX (H120, Santa Cruz Biotecnology) and Vinculin (9264, Sigma-Aldrich). Western blotting against Vinculin was performed as loading control.

Massive parallel sequencing

Genomic DNA extracted from UCDMel-ΔH cells and healthy control fibroblasts was examined using the Illumina® Clinical-Exome Sequencing TruSight One Gene Panel. This panel includes all the known disease-associated genes described in the OMIM database until 2013, and captures 62,000 exons and their flanking intronic regions. After sequencing on a Nextseq500 platform, the reads were aligned with the reference genome and the depth of coverage of the *HIF1α* gene was analyzed in order to detect genomic rearrangements.

QUANTIFICATION AND STATISTICAL ANALYSIS

Statistical details of experiments including statistical tests used, exact value of n, dispersion and precision measures (mean ± SEM) and statistical significance are reported in the Figures and Figure Legends. The differences between 2 groups with similar variances were analyzed using a two-tailed Student's t test. When the variances of the groups were significantly different, a two-tailed t test with Welch's correction was used. Differences between the variances of the groups were analyzed with the Fisher test (F-test). When more than 2 groups were analyzed, statistical analysis was performed by one-way ANOVA followed by Tukey's post hoc test. All statistical analyses were performed using GraphPad Prism software. A p value lower than 0.05 was considered significant.